Journal of Power Sources 248 (2014) 588–595

Contents lists available at SciVerse ScienceDirect

Journal of Power Sources

journal homepage: www.elsevier.com/locate/jpowsour

C/LiFePO$_4$/multi-walled carbon nanotube cathode material with enhanced electrochemical performance for lithium-ion batteries

Guohui Qin [a], Quanping Wu [b,*], Jun Zhao [b], Qianqian Ma [a], Chengyang Wang [a,c,*]

[a] School of Chemical Engineering and technology, Tianjin University, Tianjin 300072, China
[b] School of Mechanical Engineering, Tianjin University, Tianjin 300072, China
[c] Synergetic Innovation Center of Chemical Science and Engineering, Tianjin, China

HIGHLIGHTS

- C/LiFePO4/MWCNTs were prepared by a hybrid of hydrothermal progress and an electro-polymerization progress.
- The obtained C/LiFePO$_4$/MWCNTs electrode displays high-rate ability, cyclic stability and a high tap density.
- This economic, facile, and green synthesis method enables the production on a large scale.

GRAPHICAL ABSTRACT

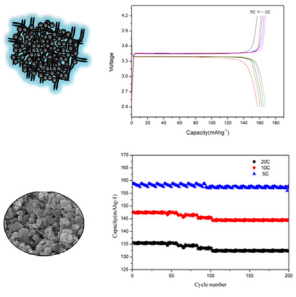

ARTICLE INFO

Article history:
Received 9 April 2013
Received in revised form
11 June 2013
Accepted 12 June 2013
Available online 21 June 2013

Keywords:
Lithium iron phosphate
Carbon network cathode
Material
Lithium-ion batteries

ABSTRACT

C/LiFePO$_4$/multi-walled carbon nanotubes composite is prepared by a hybrid of hydrothermal progress that involves an in-situ multi-walled carbon nanotubes embedding approach and a facile electro-polymerization polyaniline process. The designed material on nanosize with about 100–200 nm in length contains tridimensional networks and uniform-thickness carbon layer, which remarkably enhance its electronic conductivity. The synthesized LiFePO$_4$ composite offers a discharge capacity of 169.8 mAh g^{-1} at the C/2 rate and high capacity retention at the 5C rate. Meanwhile, the well-crystallized material composed of many densely aggregated nanoparticles and interconnected nanochannels presents a high tap density leading to excellent volumetric Li storage properties at high current rates (>135 mAh cm^{-3} at 20C), and stable charge/discharge cycle ability (>95% capacity retention after 200 charge/discharge cycles). As such, the prepared material with controllable size and structure yields an enhanced electrochemical performance in terms of charming rate capability, cycling life and capacity retention as a cathode in lithium-ion batteries, this non-organic facile synthesize avenue can be promising to prepare high-power electrode materials.

1. Introduction

The olivine structure lithium iron phosphate LiFePO$_4$ has been considered to be one of a prominent cathode electrode material alternative for Li-ion battery. It contains appealing features, including a relatively high theoretical specific capacity of 170 mAh g^{-1}, a flat voltage profile (3.4 V vs. Li$^+$/Li), high safety, high thermal stability in the charged state, as well as environmental benignity, low cost and abundant material supply. However, LiFePO$_4$ cathodes suffer from poor electronic conductivity and low ionic diffusivity leading to high initial capacity losses and poor rate capabilities which hinder its practical application [1–3]. The low energy

* Corresponding authors. Tel./fax: +86 22 27890481.
E-mail addresses: guohuiq163@sina.com (G. Qin), wqping@ustc.edu.cn (Q. Wu), cywang@tju.edu.cn (C. Wang).

0378-7753/$ – see front matter © 2013 Published by Elsevier B.V.
http://dx.doi.org/10.1016/j.jpowsour.2013.06.070

density and difficulties in electrode fabrication are other limitations of mono dispersed $LiFePO_4$ particles. The ways to overcome the limitation of lithium-ion diffusion depend mainly on downsizing and controlling the morphology of the particle to decrease length of the lithium-ion diffusion pathway inside the particle [4,5], while improvements in conductivity were commonly achieved by coating conductive coating [6,7] or cation doping [8–11]. Carbon coating based on a controlled morphology preparation method which gains nanosized particles is supposed to be the most effective and low cost way to overcome the disadvantages, because the dispersed carbon provides pathways for electron transference and the electrical contact with electrolyte solution and the decreased particle size improves the lithium-ion diffusion impedance, hence leads to a significantly improved electrochemical performance. Multi-walled CNTs (MWCNTs) providing tridimensional networks have been proven to be the most effective in reducing the resistance, and thus improving the electrochemical performance of the composite cathode [12]. More recently, the hybrid of $LiFePO_4$/MWCNTs composites was carried out for improved electrochemical performance [13–16]. It is reported that nano-$LiFePO_4$/MWCNTs cathode materials prepared by Room-Temperature Solid-State Reaction and Microwave Heating showed a high capacity and stable cycle ability [17].

Although in this work using MWCNTs is a promising way to achieve an improved conductivity and the additive of citric acid shows its advantage of improving the crystallization, hence, accelerating diffusion rates of Li ions, some other aspects of $LiFePO_4$ need to be considered in order to increase the tap density, in turn, leads to give rise to the volumetric energy density. Previous works show particularly that the morphology of nanosized $LiFePO_4$ [18,19] and the choice of the preparation route largely influence its electrochemical reactivity. It is desirable to synthesize $LiFePO_4$/MWCNTs nanosized composites by rational preparation method for both high volumetric energy density and good electrochemical performance [20].

A highly conductive $LiFePO_4$/MWCNTs composite as a high performance cathode through a hydrothermal method performs an excellent electrochemical performance as well as a high tap density [21]. Hydrothermal synthesis has been to be one of the most effective route because MWCNTs present a good contact with $LiFePO_4$ along with low energy consumption and its capability to control the size and morphology of secondary $LiFePO_4$ particles during the preparation progress. Subsequently, the conductivity of $LiFePO_4$/MWCNTs can be further improved by adding additional electrical polymer conductors, followed by a heat-treatment procedure to convert the polymer matrix into a conductive carbon. Polyaniline (PANI) has become the most attractive one because of its easy preparation, high conductivity, good environmental stability and low price of the monomer and high aspect ratio [22,23].

C/$LiFePO_4$/MWCNTs nanosized composites have been developed as a cathode material in this study. The synthesis process is illustrated in Fig. 1. Nanosized $LiFePO_4$ primary particles with a mean particle size 100–200 nm were well interconnected by MWCNTs, in which MWCNTs act as a highly conductive tridimensional network. A uniform-thickness PANI coating was deposited on top of the interconnected $LiFePO_4$ primary particles using a facile electropolymerization process after proceeded by a heat treatment. Both of them greatly enhance the conductivity of the sample. Besides, the additive of citric acid helped to form a well controlled crystallization of the hybrid composite, which is beneficial to forming high tap density, in turn, leading to a good rate performance. The nanosized $LiFePO_4$ composite performs improved conductivity, rate capabilities and a good cyclic behaviors, which is promising as a high performance cathode material for lithium-ion batteries.

2. Experimental

2.1. Functionalization of MWCNTs

The MWCNTs (FloTube9000, purity ≥ 95 wt%, 20 nm in diameter, 10 μm in length) used in this work were provided by CNano Technology Ltd. These MWCNTs are about 10–20 nm in diameter and 10–30 μm in length with an approximate surface area of 500 $m^2\ g^{-1}$. In order to increase the interfacing binding between the MWCNTs and $LiFePO_4$, MWCNTs have to be pre-treated by nitric acid for the surface functionalization [24].

Purification was firstly conducted in order to remove the catalyst, MWCNTs were immerged in diluted sulfuric acid (50 wt %) at 120 °C for 5 h. Subsequently, MWCNTs were filtered by using glass

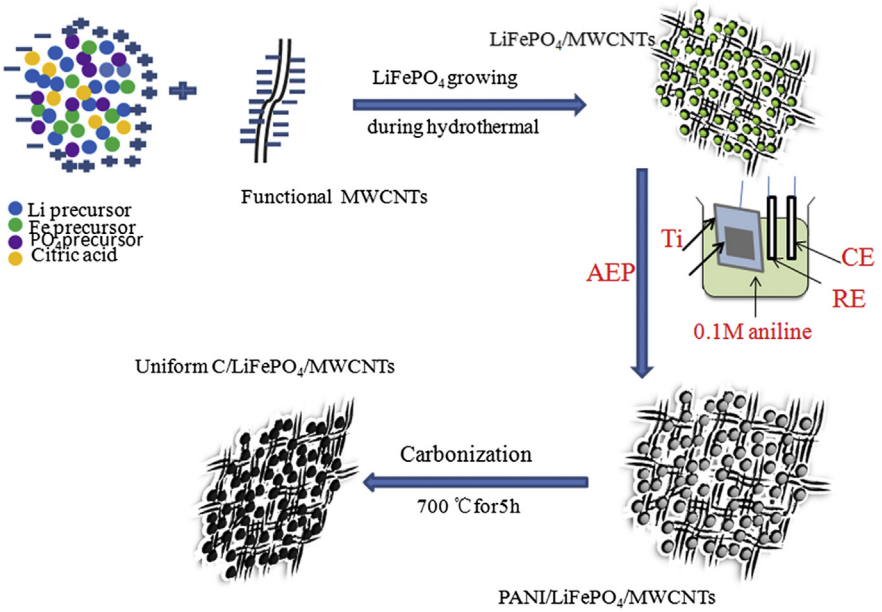

Fig. 1. Schematic illustration of the synthesis procedure of C/$LiFePO_4$/MWCNTs nanosized particles.

frit, washed with distilled water, and dried at 120 °C for 12 h. Functionalized MWCNTs were prepared according to the previous work [25]. First, 0.01 g of purified MWCNTs were oxidized in 100 mL of HNO_3 and H_2SO_4 mixture (1:3 by volume) solution by refluxing at 70 °C for 8 h and sonicated for 4 h to perform a partial oxidation of the surface and the formation of oxidized groups such as C–OH–, –O–C=O or C=O. Finally, the solution was filtered by vacuum filtration through a poly(tetrafluoroethylene) (PTFE) filter (Millipore, 25 mm in diameter, 0.2 μm pores) and washed with distilled water.

2.2. Preparation of C/$LiFePO_4$/MWCNTs

C/$LiFePO_4$/MWCNTs composite was prepared as cathode materials for lithium-ion batteries. Firstly, the nanosized $LiFePO_4$/MWCNTs composite with tridimensional networks embedded was prepared by the in-situ hydrothermal growth. The stoichiometric amounts of $FeSO_4 \cdot 7H_2O$, LiOH and H_3PO_4 corresponding to 0.01 mol of $LiFePO_4$ were dissolved in 50 mL of distilled water under magnetic stirring. 0.01 mol of citric acid was dissolved in the mixture. Subsequently, 0.039 g pre-treated MWCNTs were dispersed into the solution under ultrasonication. Finally, the resulting mixture was poured into a sealed Teflon-lined stainless steel autoclave and heated at 180 °C for 5 h, the preparation of pure $LiFeO_4$ was the same as the above procedure except without the additive of MWCNTs and citric acid. All procedures were performed under N_2 atmosphere for the sake of avoiding the oxidation of Fe^{2+} ion.

In order to further improve the conductivity of the $LiFePO_4$/MWCNTs composite, a uniform-thickness PANI layer by using an anodic electro-polymerization (AEP) process was uniformly coated onto their surface to form a homogenous PANI/$LiFePO_4$/MWCNTs composite. The in-situ AEP process was conducted at a constant potential of 1 V for 600 s in a three-electrode cell at room temperature. The $LiFePO_4$/MWCNTs composite was dispersed into ethanol and the solution was applied onto a titanium substrate to play a role of the working electrode. The PANI monomer (0.1 mol L^{-1}) in sulfuric acid (0.1 mol L^{-1}) was drafted as the electrolyte; and Hg/$HgSO_4$ and Pt mesh were designed as the reference and counter electrodes, respectively. After washing with distilled water and acetone several times, the collected PANI/$LiFePO_4$/MWCNTs composites were calcined at 700 °C for 5 h in a tubular furnace under a N_2 ambient to gain the interconnected carbon shell on the surface of $LiFePO_4$/MWCNTs composite, restricting the in-situ crystallite growth of $LiFePO_4$.

2.3. Characterizations

The X-ray diffraction (XRD) patterns of $LiFePO_4$ samples were obtained using a PANalytical X-pert diffractometer (PANalytical, Netherlands) with a Cu Kα radiation operated at 40 kV and 30 mA. Raman spectrum was measured by a Renishaw in ViaRaman microscope at room temperature with the 532 nm line of an Ar ion laser as an excitation source. X-ray photoelectron spectroscopy (XPS, VGMicro Tech) was used to measure the oxygen content in the functionalized MWCNTs. Morphology and structure of the samples were analyzed via field-emission scanning electron microscopy (FE-SEM, S4800, Thermo Fisher) and high-resolution transmission electron microscopy (HR-TEM, Tecnai G2F20, Philips).

The electrochemical performance of the $LiFePO_4$ samples was tested using a CR2025-type coin cell. To prepare the working electrodes, the active material powder, carbon black and poly(-vinylidene fluoride) binder were mixed at a weight ratio of 80:10:10 in N-methyl-2-pyrrolidone solvent. The mixed viscous slurry was coated onto Al foil and dried at 120 °C under vacuum for 12 h. The obtained film was cut into circular discs with an area of ~1.5 cm^2, and the discs were pressed at a pressure of 10 MPa to act as the working electrodes. The positive electrodes with approximately 2.3 mg of the active materials with a uniform thickness were assembled in coin cells with a lithium metal foil as the negative electrode, a Celgard 2400 film as the separator, and 1.0 M $LiPF_6$ solution in ethylene carbonate, diethyl carbonate and dimethyl carbonate (1:1:1, in volume) as the electrolyte. The electrode performance was investigated in terms of cyclic voltammetry curve, charge/discharge curves and cycling capacity using a NEWARE battery-testing system (Neware Co., Ltd., China) at the cut-off voltages of 2.5 and 4.2 V. Electrochemical impedance spectroscopy (EIS) was measured using CHI604D (CH Instruments, China). EIS measurements were carried out in the frequency range from 1 mHz to 1 MHz with an AC voltage signal of ±5 mV. All the electrochemical measurements were carried out at room temperature, and the potentials were given with respect to Li^+/Li.

3. Results and discussion

3.1. Structure and morphology

XRD was used to detect the crystallinity information of the as prepared pristine $LiFePO_4$, $LiFePO_4$/MWCNTs and C/$LiFePO_4$/MWCNTs nanosized particles (Fig. 2), confirming the formation of $LiFePO_4$. The lattice parameters of all samples are the same to those given in the ICDD card (No. 96-110-1112) [26]. Calculation of the pattern gave the lattice parameter values of a = 5.9434 Å, b = 10.3045 Å, c = 4.6859 Å and a unit cell volume of 286.95 $Å^3$, which were in good agreement with the literature values [27,28].

From Fig. 2, it is also drawn that pure $LiFePO_4$ composites show broader olivine peaks with lower intensities, as compared with the modified samples. This is because the presence of MWCNTs and citric acid regulate the crystal-growth rate during heat treatment. Well symmetric peak suggests the good crystallinity of the modified sample.

MWCNTs alone exhibited diffraction peak corresponding to the (002) reflection at ~26.0, they were not distinctively detected in the pattern of all the $LiFePO_4$ samples, which was probably due to the low MWCNTs content. The carbon was in low content, so that no diffraction peak of carbon in XRD pattern was detected. However, Raman shift, evidencing the presence of carbon in the carbon-coated $LiFePO_4$ composites Fig. 3(a). In Fig. 3(a), the strong peaks at

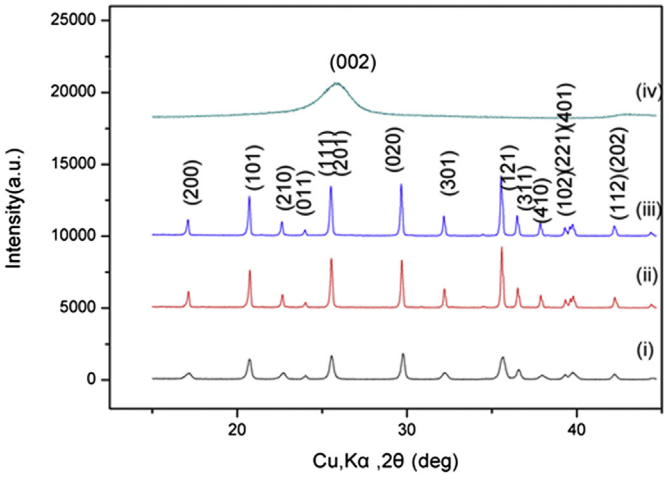

Fig. 2. XRD patterns of (i) pristine $LiFePO_4$ powder, (ii) $LiFePO_4$/MWCNTs composite, (iii) C/$LiFePO_4$/MWCNTs material and (iv) MWCNTs.

1342 and 1573 cm^{-1} are ascribed to D-band and G-band respectively. The G-band stands for the presence of graphite carbon, whereas D-band is attributed to disorders or defects in the graphite structure [29]. The intensity ratio of D and G bands (I_D/I_G) is used to evaluate the disorder in the materials. The ratios I_D/I_G for $LiFePO_4$/MWCNTs and C/$LiFePO_4$/MWCNTs are 0.99 and 0.75, respectively. The higher I_D/I_G ratio implies more defects of the $LiFePO_4$/MWCNTs samples, demonstrating that the presence of MWCNTs helps to create ordered carbon and the load of uniform-thickness PANI further improve the disorder of C/$LiFePO_4$/MWCNTs to some extent.

Responsibly, in Fig. 3(b), large amounts of oxygenated groups, hydroxyl, carbonyl and carboxyl groups were observed on the functionalized MWCNTs surface, indicting the strong chemical reactivity between $LiFePO_4$ and MWCNTs. The low carbonization temperature in the hydrothermal process allowed the further functionalization of MWCNTs. With oxygenated groups and the aid of a chelating agent citric acid, the $LiFePO_4$ particles and MWCNTs in excellent interface binding were uniformly interconnected, which is further confirmed by SEM images of $LiFePO_4$ materials (Fig. 4).

The carbon contents of modified products were measured by using elemental analysis and they were found to be 3.6% and 5.9 wt %, respectively, for $LiFePO_4$/MWCNTs composite, and C/$LiFePO_4$/MWCNTs sample. The low carbon content is beneficial to increasing its tap density and makes it more promising in industrial production and application. The tap density of the prepared C/$LiFePO_4$/MWCNTs and $LiFePO_4$/MWCNTs reached 1.60 g cm^{-3} and 1.61 g cm^{-3}, respectively, which was slightly lower than that of the pure $LiFePO_4$ composite (1.63 g cm^{-3}) because of the addition of carbon. The higher tap density of cathode material pronouncedly makes a significantly higher volumetric energy density. In addition, the interconnected three-dimensional networks and the overall carbon coating are good for the electrical conductivity of the C/$LiFePO_4$/MWCNTs particles.

The electrical conductivity of the C/$LiFePO_4$/MWCNTs material measured by a four-point probe method was 2.3×10^{-1} S cm^{-1}, which was 8.2 times higher than that for pristine $LiFePO_4$ (2.8×10^{-2} S cm^{-1}) and 2.8 times higher than that of the $LiFePO_4$/MWCNTs (8.1×10^{-2} S cm^{-1}), clearly showing that the electrical conductivity of C/$LiFePO_4$/MWCNTs nanosized particles is remarkably enhanced by the incorporation of interwaved network and the uniform load of PANI carbon layer.

Fig. 4 shows typical SEM images of pristine $LiFePO_4$ composites and modified $LiFePO_4$ particles. The modified $LiFePO_4$ composite contains well-crystallized and densely aggregated nanoparticles with interconnected nanochannels, which give rise to a high tap density. MWCNTs and citric acid were responsible for the formation of nanosized morphology during the hydrothermal process. Compared with the SEM spectrum, Fig. 4(a)–(c), it is find that citric acid helping to decease the packing density of each sample regulate and control the homogenous distribution of $LiFePO_4$, while MWCNTs functioned as a lead and well connected the $LiFePO_4$ particles. Modified $LiFePO_4$ particles are well-mixed on nanosize with about 100–200 nm in length. MWCNTs can be observed on $LiFePO_4$ platelet particles clearly and interlaced particles together to form a carbon nano-network which leads to electronic continuity between particles, these interconnected nanochannels allow the liquid electrolyte to penetrate in all directions inside the particles. Interconnected with MWCNTs without noticeable aggregation and then was coated by PANI carbon layer after the carbonization at 700 °C, the particles of C/$LiFePO_4$/MWCNTs is homogenous, which is more beneficial to the rate capability of cathode materials.

High-resolution TEM images of the $LiFePO_4$ particles in Fig. 5 also verify that samples added citric acid alleviates the aggregation and modified $LiFePO_4$ samples are more well-crystallized, which have been proven by the XRD and SEM results. A thin carbon layer with a thickness in the range of 1–3 nm was coated into the $LiFePO_4$ particles, which was classified to be effective in achieving optimized rate capabilities. With a thicker carbon coating, the reversible capacity tended to decrease partly because of the increasingly hindered electrolyte transport [30].

3.2. Electrochemical performance of $LiFePO_4$ composites

Cyclic voltammetry was conducted in order to investigate the effect of the electrochemical properties of the $LiFePO_4$ samples by using a scanning rate of 0.1 mV s^{-1}, voltage range: 2.4–4.2 V. Fig. 6 compared the CV profiles of pristine $LiFePO_4$, $LiFePO_4$/MWCNTs and C/$LiFePO_4$/MWCNTs in the first cycle. The CV of C/$LiFePO_4$/MWCNTs material presents the most symmetrical and sharper shape of the anodic/cathodic peaks, the well-defined peaks and narrower peak separation indicate the higher electrochemical reactivity of modified $LiFePO_4$ composites [31], a reflection of small polarization, high Li-ion diffusion rate and low inner resistance. Lithium-ion intercalation/deintercalation reactions, accompanied by electron removal, essentially depend on electronic conducting. The additive of MWCNTs and PANI greatly improves the conductivity of C/$LiFePO_4$/MWCNTs, in turn, leads to the most active in redox

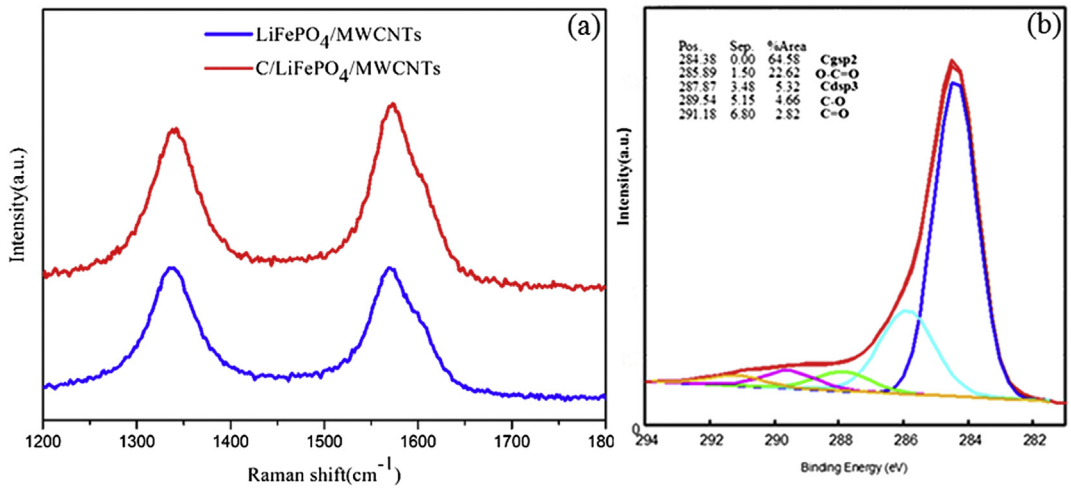

Fig. 3. (a) Raman spectra of $LiFePO_4$/MWCNTs and C/$LiFePO_4$/MWCNTs samples and (b) deconvoluted C1s spectra of functionalized MWCNTs.

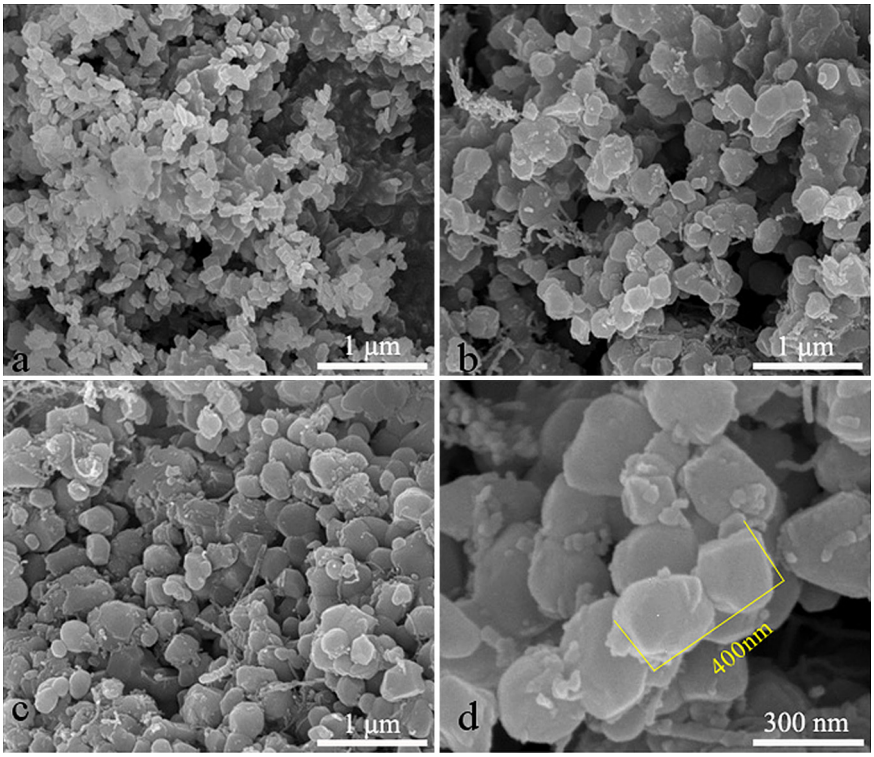

Fig. 4. SEM image of (a) pristine $LiFePO_4$ sample, (b) $LiFePO_4$/MWCNTs composite, (c) and (d) C/$LiFePO_4$/MWCNTs material at various magnifications.

reactions. Besides, lithium ions and electrons were quite active in the regard, which could be partly derived from the uniform smaller nanosized particles that reduced the diffusion length of the lithium ions in $LiFePO_4$ and facilitated reversible electrochemical reactions during extraction and insertion of lithium ions.

In addition, the diffusion of lithium ions in the solid state, depending on the contact area, is considered to be the slowest process that can be improved by increasing the surface area [32]. The specific BET surface area of the C/$LiFePO_4$/MWCNTs is 21.6 $m^2\ g^{-1}$, for $LiFePO_4$/MWCNTs and $LiFePO_4$, the surface area is 19.4 and 10.6 $m^2\ g^{-1}$, respectively. The incorporation of MWCNTs and PANI carbon layer can greatly enhance the surface area of $LiFePO_4$, giving rise to good electrolyte infiltration and favoring the diffusion kinetics of lithium ions to some extent.

Broadened peaks of pristine $LiFePO_4$ present poor kinetics, lithium intercalation and deintercalation is sluggish, while sharp peaks of C/$LiFePO_4$/MWCNTs highlights excellent kinetics [33,34], lithium intercalation and deintercalation is facile. The comparison indicated that the added citric acid, MWCNTs and overall carbon distribution could effectively improve the electrochemical performance. Citric acid addition helped to form well-crystallized nanosized particles and shorten the diffusion path of lithium ions, while the continuous carbon layers which wrap homogeneously around the surface of $LiFePO_4$ nanoparticles are served as a fast path for electron migration during charge/discharge processes. Good electrical conductivity, good electrochemical reversibility, high stability, and high electronic conductivity in the doped state make it an excellent material for electrical applications.

Fig. 7 shows the initial charge–discharge curves of all samples. The voltage plateaus at the range of 3.3–3.5 V which corresponds to the Fe^{3+}/Fe^{2+} redox couple due to Li extraction, indicated the lithium extraction and insertion reactions of $LiFePO_4$ particles. It is noted the voltage plateau is lengthened for the MWCNTs modified $LiFePO_4$ materials, which should be attributed to the higher electrochemical reactivity of modified $LiFePO_4$ and excellent kinetics. This result is in accordance with the CV profiles. The modified

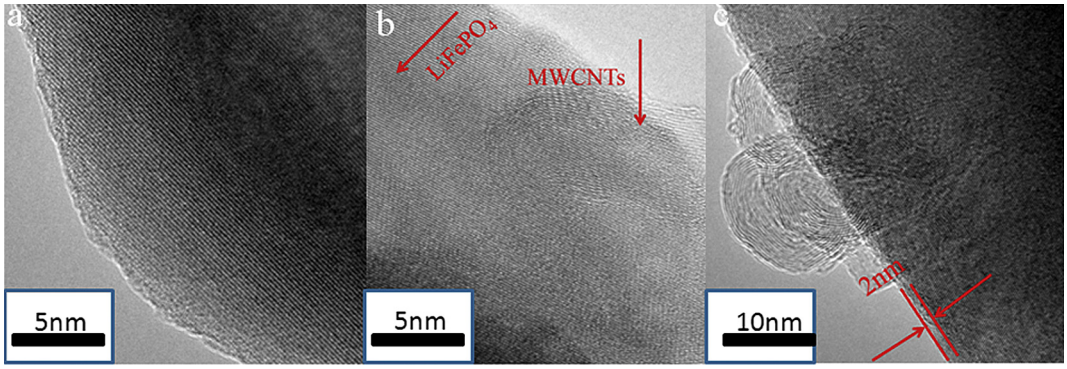

Fig. 5. TEM image of (a) pristine $LiFePO_4$ sample, (b) $LiFePO_4$/MWCNTs composite and (c) C/$LiFePO_4$/MWCNTs sample.

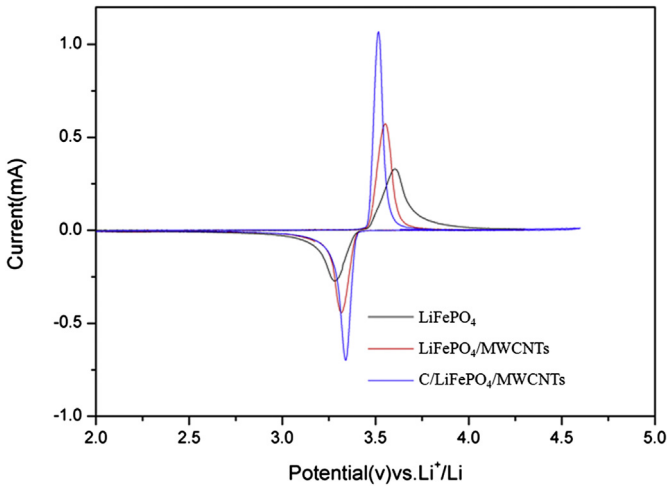

Fig. 6. Cyclic voltammetry curves of the $LiFePO_4$ samples.

$LiFePO_4$ materials exhibit higher capacities than pure $LiFePO_4$ at a low rate C/2, and a maximum capacity of 169.8 mAh g^{-1}(nearly to its theoretical capacity 170 mAh g^{-1}) are found in C/$LiFePO_4$/MWCNTs, while that of the MWCNTs/$LiFePO_4$ and the pure $LiFePO_4$ just reach 158.1 and127.2 mAh g^{-1}, respectively. Meanwhile, the gap between the charge and discharge voltage plateau is very small. The high-discharge capacity of C/$LiFePO_4$/MWCNTs was presumed to be associated with a fast reaction and ionic diffusion kinetics of C/$LiFePO_4$/MWCNTs nanosized particles, good electronic contact by retaining the ability to coat individual nanoparticles with the tridimensional networks and overall carbon coating, which coincide with the aforementioned CV result.

In order to investigate the rate performance of all samples, the charge/discharge curves at higher rates from 1C to 5C were shown in Fig. 8(a)–(c). Accordingly, the dependence of specific capacity on current density was shown in Fig. 8(d). At 1C, the C/$LiFePO_4$/MWCNTs nanosized particles displayed a discharge capacity of 167.5 mAh g^{-1} at 1C, which was higher than that of the $LiFePO_4$/MWCNTs (155.3 mAh g^{-1}). At higher rates, the outstanding capacity performance of the C/$LiFePO_4$/MWCNTs particles was even more obvious. Its discharge capacity at 5C was still over 157.5 mAh g^{-1}, whereas that for $LiFePO_4$/MWCNTs was just 110 mAh g^{-1}. As to pure $LiFePO_4$, the capacity decreased to 95 mAh g^{-1} at 3C with a serious

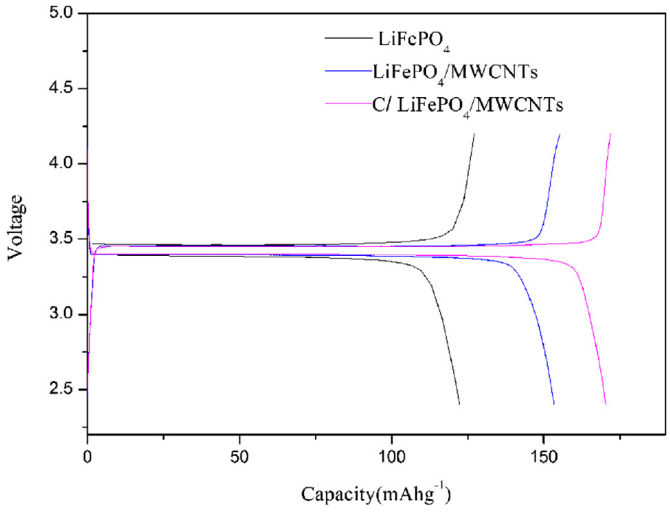

Fig. 7. Initial voltage vs. capacity curves of the $LiFePO_4$ samples at C/2.

polarization tendency, while the modified samples proned to slight polarization phenomenon. The tridimensional networks and full carbon coatings throughout the modified $LiFePO_4$ powder ensure transfer electrons through all directions and mitigate the polarization. The capacity fading could be attributed to the slow diffusion of lithium-ion in $LiFePO_4$ and the poor contact between the $LiFePO_4$ particles and conductors.

With increasing rate, the potential plateau for C/$LiFePO_4$/MWCNTs remains flat, even though becomes slightly shorter, while that of pristine $LiFePO_4$ and $LiFePO_4$/MWCNTs become shorter and bends down gradually, especially for pristine $LiFePO_4$. The gap between the charge and discharge voltage plateau decreases from 0.5 to 0.2 V at 10C, indicating that the polarization decreases by MWCNTs and PANI carbon layer modification and that the rate capability of C/$LiFePO_4$/MWCNTs is improved, which is consistent with the CV and initial charge–discharge curves.

The cycle performances of modified samples were extensively explored from 1C to 5C in Fig. 9(a). As shown in Fig. 9(a), the $LiFePO_4$/MWCNTs and C/$LiFePO_4$/MWCNTs samples have a stable cycle performance at these rates. Enhanced conductivity by tridimensional networks and continuous carbon load together with the moderate nanosized particle size enhances the cycle efficiency of $LiFePO_4$ due to their prevention of the irreversible reactions and electron transport [35], coinciding with the galvanostatic charge and discharge profiles result. More importantly, C/$LiFePO_4$/MWCNTs exhibit an excellent cycle and rate performance with no significant fade compared with the $LiFePO_4$/MWCNTs at all current density.

As with the high reversible capacity of an electrode material, high-rate performance is also of importance for the increasing demand of lithium-ion battery applications. The C/$LiFePO_4$/MWCNTs sample in the long-term cycling at higher current rates was undertaken in the following progress. As shown in Fig. 9(b), the nanosized C/$LiFePO_4$/MWCNTs particles still delivered a discharge capacity of 132.2 mAh g^{-1} at the 20C rate after 200 cycles, corresponding to 97.4% of the capacity retention, 144.3 mAh g^{-1} at 10C with 98.8% of the capacity retention, 157.4 mAh g^{-1} at 5C rate with 99.1% capacity retention. These are among the best rate capabilities reported for $LiFePO_4$/C systems [36,37].

The cathode discharge capacity remained virtually unchanged after 200 cycles, indicating highly reversible lithium insertion/extraction kinetics. The structural integrity of the C/$LiFePO_4$/MWCNTs nanosized particles was maintained even after high-rate charge and discharge, implying that the structural robustness of the well-crystallized $LiFePO_4$ nanoparticles. The C/$LiFePO_4$/MWCNTs material with outstanding stability supplies a platform to realize high-power applications in lithium-ion batteries.

To provide more information about the $LiFePO_4$ samples for the electrochemical property, AC impedance measurements are performed on all the samples at the charged state after cycling (Fig. 10). As depicted in Fig. 10, these impedance spectra combined of a depressed semicircle in the high frequency region and a straight line in the low-frequency region. The semicircle is mainly related to the charge-transfer resistance and the corresponding capacitances at the electrode/electrolyte interface, the straight line in the low-frequency region has to do with the diffusion behavior of lithium ions within the $LiFePO_4$ particles [38,39].

The charge-transfer resistance was calculated from the semicircle in the high-middle frequency range as about 90 Ω, 60 Ω and 40 Ω for the pristine $LiFePO_4$, $LiFePO_4$/MWCNTs and C/$LiFePO_4$/MWCNTs, respectively, indicating that charge transfer from the electrolyte to active materials is obviously accelerated by tridimensional networks and the overall carbon coating at the interface between $LiFePO_4$ and electrolyte. The bigger slope of impedance of modified $LiFePO_4$ samples indicates their higher electrochemical activity, which ascribed to the small grain size and short diffusion

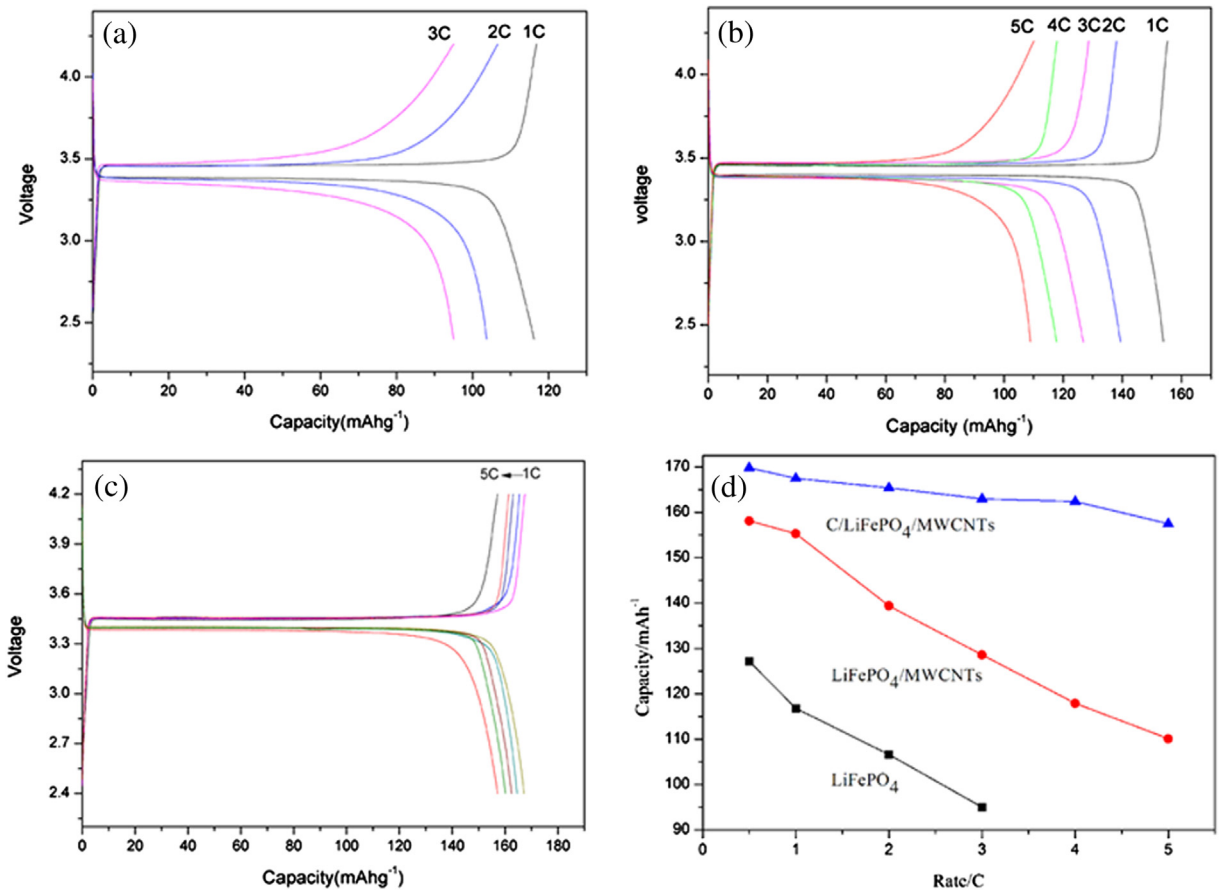

Fig. 8. Charge/discharge curves of (a) pristine $LiFePO_4$ sample, (b) $LiFePO_4$/MWCNTs composite, (c) C/$LiFePO_4$/MWCNTs sample, and (d) the dependence of specific capacity on current density.

path of lithium ion. The improved lithium-ion diffusion process within C/$LiFePO_4$/MWCNTs particles estimated from the oblique line at low frequencies is greatly enhanced by tridimensional networks allowing uniform carbon coating and electrolyte penetration, improving the electronic conductivity and reducing the diffusion path of the lithium ions. Those results are in agreement with the CV profiles, rate performance and cycling behavior results.

According to the above discussion, such an attractive high performance of C/$LiFePO_4$/MWCNTs can be derived from well-mixed conducting materials, interconnected tridimensional nanonetworks and well crystallization. The effective dispersion of three-dimensional network and uniform carbon layer not only allow better penetration of electrolyte to promote lithium-ion diffusion but also increase the electrochemical reaction surface, thus ultimately alleviate electrode polarization, simultaneously, provide a good stability and capacity retention. The well-crystallized and nanoembossed nanoparticles present a high tap density, in turn, develop a high-rate capability.

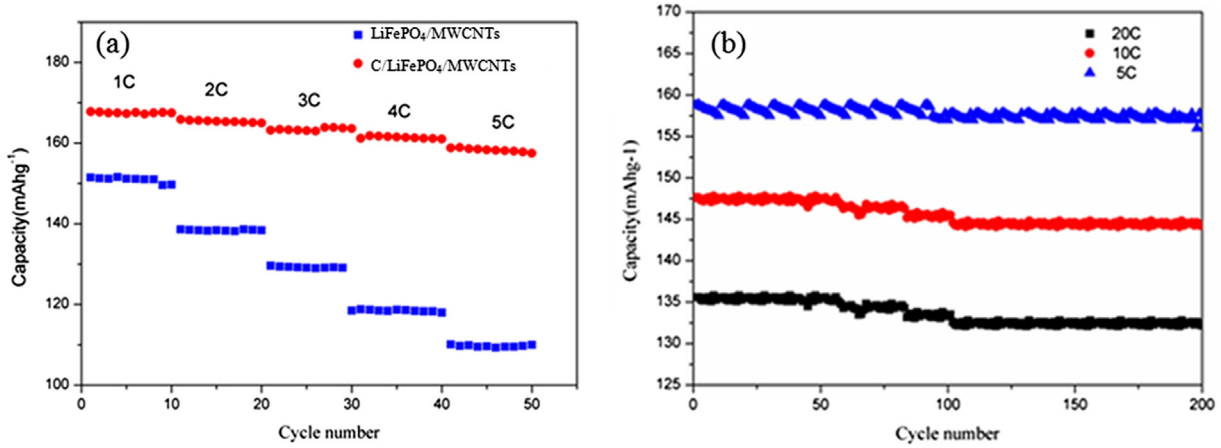

Fig. 9. The rate performances of (a) MWCNTs modified $LiFePO_4$ materials at various current rates, (b) long-term stability for C/$LiFePO_4$/MWCNTs material at high current rates.

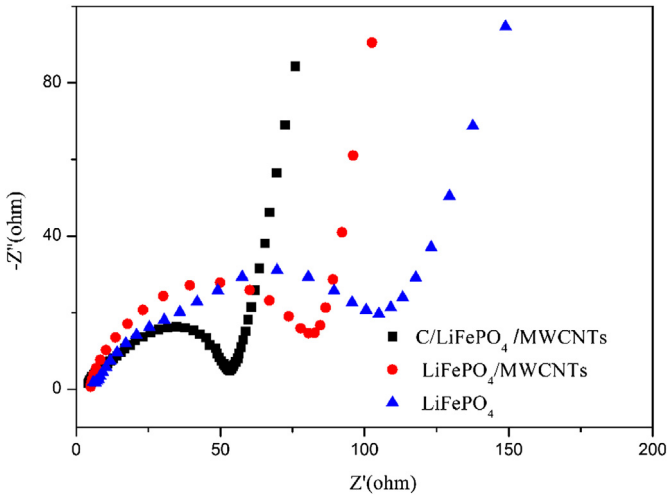

Fig. 10. Electrochemical impedance spectroscopy (EIS) result of the $LiFePO_4$ samples.

4. Conclusions

In summary, C/$LiFePO_4$/MWCNTs nanosized composite has been successfully synthesized by using a combination of hydrothermal and electro-polymerization techniques. Favorable lithium-ion transport and electron transfer highways built from the effective continuous carbon network which bridges the $LiFePO_4$ particles enhancing the electron conductivity within the secondary particles are observed. In addition, the composite possesses a high tap density. Thus, combining by improved electronic conductivity and high tap density, tremendously improved electrochemical performance including high volumetric energy density, excellent cyclic behavior and rate capacity are achieved. These excellent electrochemical performances provide that the nanosized particles can be promising for high-power lithium-ion batteries and this economic, facile, and green synthesis method supplies a platform to realize a large scale in industry.

Acknowledgment

The authors thankfully acknowledge the support of the Natural Science Foundation of Tianjin City (No. 12JCZDJC27000) for financial supports.

References

[1] X.M. Lou, Y.X. Zhang, J. Mater. Chem. 21 (2011) 4156.
[2] J.F. Qian, M. Zhou, Y.L. Cao, X.P. Ai, H.X. Yang, J. Phys. Chem. C 114 (2010) 3477.
[3] F. Yu, J.J. Zhang, Y.F. Yang, G.Z. Song, J. Power Sources 195 (2010) 6873.
[4] A. Yamada, S.C. Chung, K. Hinokuma, J. Electrochem. Soc. 148 (2001) 224–229.
[5] P.P. Prosini, M. Carewska, S. Scaccia, P. Wisniewski, M. Pasquali, Electrochim. Acta 48 (2003) 4205–4211.
[6] L.N. Wang, Z.G. Zhang, K.L. Zhang, J. Power Sources 167 (2007) 200–205.
[7] K. Kim, J.-H. Jeong, I.-J. Kim, H.-S. Kim, J. Power Sources 167 (2007) 524–528.
[8] P. Subramany Herle, B. Ellis, N. Coombs, L.F. Nazar, Nat. Mater. 3 (2004) 147–152.
[9] K.S. Park, J.T. Son, H.T. Chung, S.J. Kim, C.H. Lee, K.T. Kang, H.G. Kim, Solid State Commun. 129 (2004) 311.
[10] J.B. Heo, S.B. Lee, S.H. Cho, J. Kim, S.H. Park, Y.S. Lee, Mater. Lett. 63 (2009) 581–583.
[11] E.M. Jin, B. Jin, D.-K. Jun, K.-H. Park, H.-B. Gu, K.-W. Kim, J. Power Sources 178 (2008) 801–806.
[12] G. Wang, Q. Zhang, Z. Yu, M. Qu, Solid State Ionics 179 (2008) 263–268.
[13] X.L. Li, F.Y. Kang, X.D. Bai, W. Shen, Elecrochem. Commun. 9 (2007) 663.
[14] L. Wang, Y.D. Huang, R.R. Jiang, D.Z. Jia, J. Electrochem. Soc. 154 (2007) A1015.
[15] T. Muraliganth, A.V. Murugan, A. Manthiram, J. Mater. Chem. 18 (2008) 5661.
[16] E. Avci, M. Mazman, D. Uzun, E. Biçer, T. Sener, J. Power Sources 240 (2013) 328–337.
[17] X.L. Li, F.Y. Kang, X.D. Jiang, D.Z. Jia, J. Electrochem. Soc. 11 (2007) A1015–A1019.
[18] C.M. Doherty, R.A. Caruso, B.M. Smarsly, P. Adelhelm, C. Drummond, J. Chem. Mater. 21 (2009) 5300–5306.
[19] X.L. Wu, L.Y. Jiang, F.F. Cao, Y.G. Guo, L.J. Wan, Adv. Mater. 21 (2009) 1–5.
[20] M. Chen, C.Y. Du, B. Song, K. Xiong, G.P. Yin, P. Zuo, X.Q. Cheng, J. Power Sources 223 (2013) 100–106.
[21] Z.D. Huang, S.W. Oh, Y.B. He, B. Zhang, Y. Yang, Y.W. Mai, J.K. Kim, J. Mater. Chem. 22 (2012) 19643–19645.
[22] Q. Wang, Q. Yao, J. Chang, L.D. Chen, J. Mater. Chem. 22 (2012) 17612–17618.
[23] Z.Q. Jiang, Z.J. Jiang, J. Alloy. Compd. 537 (2012) 308–317.
[24] Y.Y. Liu, C.B. Cao, J. Li, Electrochim. Acta 55 (2010) 3921–3926.
[25] Q. Zhang, Z. Chang, M. Zhu, X. Mo, D. Chen, Nanotechnology 18 (2007) 115611.
[26] V.A. Streltsov, E.L. Belokoneva, V.G. Tsirelson, N.K. Hansen, Acta Crystallogr. Sect. B 49 (1993) 147–153.
[27] X. Wu, L. Jiang, F. Cao, Y. Guo, L. Wan, Adv. Mater. 21 (2009) 2710–2714.
[28] J. Zheng, X. Li, Z. Wang, H. Guo, S. Zhou, J. Power Sources 184 (2008) 574–577.
[29] J.L. Yang, J.J. Wang, X.F. Li, D.N. Wang, J. Liu, G.X. Liang, M. Gauthier, Y.L. Li, D.S. Geng, R.Y. Lia, X.L. Sun, J. Mater. Chem. 22 (2012) 7537–7543.
[30] R. Dominko, M. Bele, M. Gaberscek, M. Remskar, D. Hanzel, S. Pejovnik, J. Jamnik, J. Electrochem. Soc. 152 (2005) A607.
[31] C. Delacourt, C. Wurm, L. Laffont, Solid State Ionics 177 (2006) 340.
[32] S.S. Zhang, J.L. Allen, K. Xu, T.R. Jow, J. Power Sources 147 (2005) 234.
[33] H. Liu, C. Li, H.P. Zhang, L.J. Fu, Y.P. Wu, H.Q. Wu, J. Power Sources 159 (2006) 717.
[34] L. Ji, Y. Yao, O. Toprakci, Z. Lin, Y. Liang, Q. Shi, A.J. Medford, C.R. Millns, X.J. Zhang, J. Power Sources 195 (2010) 2050–2056.
[35] J.J. Wang, X.L. Sun, Energy Environ. Sci. 5 (2012) 5163–5185.
[36] X.-L. Wu, L.-Y. Jiang, F.-F. Cao, Y.-G. Guo, L.-J. Wan, Adv. Mater. 21 (2009) 2170.
[37] J. Liu, E.C. Thomas, X.Y. Song, M.D. Marca, J.R. Richardson, Energy Environ. Sci. 4 (2011) 885–888.
[38] J.Y. Xiang, J.P. Tu, L. Zhang, X.L. Wang, Y. Zhou, Y.Q. Qiao, Y. Lu, J. Power Sources 195 (2010) 8331–8335.
[39] T. Muraliganth, A. Murugan, A. Manthiram, J. Mater. Chem. 18 (2008) 5661–5668.